MDPI

Article

Ti$_2$O$_3$/TiO$_2$-Assisted Solar Photocatalytic Degradation of 4-tert-Butylphenol in Water

Saule Mergenbayeva [1] , **Timur Sh. Atabaev** [2] **and Stavros G. Poulopoulos** [1,*]

1   Department of Chemical and Materials Engineering, School of Engineering and Digital Sciences, Nazarbayev University, 53 Kabanbay Batyr Ave., Nur-Sultan 010000, Kazakhstan; saule.mergenbayeva@nu.edu.kz
2   Department of Chemistry, School of Sciences and Humanities, Nazarbayev University, Nur-Sultan 010000, Kazakhstan; timur.atabaev@nu.edu.kz
*   Correspondence: stavros.poulopoulos@nu.edu.kz; Tel.: +7-7172-694608

Abstract: Colored Ti$_2$O$_3$ and Ti$_2$O$_3$/TiO$_2$ (mTiO) catalysts were prepared by the thermal treatment method. The effects of treatment temperature on the structure, surface area, morphology and optical properties of the as-prepared samples were investigated by XRD, BET, SEM, TEM, Raman and UV–VIS spectroscopies. Phase transformation from Ti$_2$O$_3$ to TiO$_2$ rutile and TiO$_2$ anatase to TiO$_2$ rutile increased with increasing treatment temperatures. The photocatalytic activities of thermally treated Ti$_2$O$_3$ and mTiO were evaluated in the photodegradation of 4-tert-butylphenol (4-t-BP) under solar light irradiation. mTiO heated at 650 °C exhibited the highest photocatalytic activity for the degradation and mineralization of 4-t-BP, being approximately 89.8% and 52.4%, respectively, after 150 min of irradiation. The effects of various water constituents, including anions (CO_3^{2-}, NO$_3$, Cl and HCO_3^-) and humic acid (HA), on the photocatalytic activity of mTiO-650 were evaluated. The results showed that the presence of carbonate and nitrate ions inhibited 4-t-BP photodegradation, while chloride and bicarbonate ions enhanced the photodegradation of 4-t-BP. As for HA, its effect on the degradation of 4-t-BP was dependent on the concentration. A low concentration of HA (1 mg/L) promoted the degradation of 4-t-BP from 89.8% to 92.4% by mTiO-650, but higher concentrations of HA (5 mg/L and 10 mg/L) had a negative effect.

Keywords: 4-tert-butylphenol; solar photocatalysis; Ti$_2$O$_3$/TiO$_2$; degradation; mineralization

1. Introduction

Water pollution by a broad category of organic pollutants is a rising issue of worldwide concern [1]. During the last decade, the consumption of personal care products (PPCPs), pharmaceuticals and endocrine-disrupting compounds (EDCs) has increased owing to economic development and population growth [2–5]. Their widespread use has increased their appearance in the aqueous environment, including rivers, lakes and reservoirs, at concentrations starting from several nanograms (ng/L) to several micrograms (μg/L) per liter [6–12]. They can even escape wastewater treatment plants (WWTPs) and drinking water treatment plants (DWTPs), ultimately reaching drinking water sources. These contaminants are termed emerging pollutants (EPs) and can cause severe adverse effects on human health and the aquatic environment [13].

In particular, 4-t-BP is an industrial chemical used as a raw material for the production of synthetic phenol and polycarbonate resins [14,15]. As a representative of EDCs, 4-t-BP has a high estrogenic effect and acute/chronic environmental toxicity [16,17]. Considering its adverse effects on human health and aquatic systems, 4-t-BP, as a highly persistent pollutant, needs to be controlled efficiently.

To date, various methods have been investigated to remove 4-t-BP from water, mainly including advanced oxidation processes (AOPs) and biological processes [16,18–20]. Among them, AOPs have attracted great attention for the removal such contaminants by converting

them into carbon dioxide and water [21,22]. The high efficiency of the process has mostly been associated with the production of hydroxyl radicals (standard potential, 2.8 V) used as oxidants. AOPs may vary in terms of work conditions, used materials and different paths of hydroxyl radical (OH·) production [23,24]. Heterogeneous photocatalysis may be considered an economically feasible solution to remove 4-t-BP from water due to the competitive cost of the process and the ambient conditions of temperature and pressure [25–27]. Moreover, it is considered an environmentally friendly oxidation process since it allows not only the degradation of the pollutant from the contaminated system but also its total elimination, without generating any undesired by-products, which could be even more toxic compounds than the parent one [28,29].

Although various photoactive materials have been investigated, TiO_2-based photocatalysts remain the most studied ones due to their high photocatalytic oxidation activity, chemical stability and availability [30–32]. The P25 form of TiO_2 is one of the most effective photocatalytic materials, which can be attributed to the combination of anatase and rutile phases [33–35]. However, the high energy band gap of approximately 3.0–3.2 eV limits the application of TiO_2 under solar light. In this context, numerous strategies have been devoted to extending the absorption wavelength to the visible area for the efficient utilization of sunlight. For example, the introduction of Ti^{3+} into TiO_2 demonstrated the capacity to extend the light response of TiO_2. It has been reported that the formation of Ti^{3+} species is accompanied by the generation of oxygen vacancies (O_v), which can favor the separation of electron–hole pairs and thus improve the visible light activity of TiO_2 [36–38]. Moreover, Ti^{3+} and oxygen vacancies can form localized states below the conduction band (CB), which reduces the band gap of TiO_2 (Figure 1), so that it can distinctly expand the absorption to the visible region [39–43]. The reported methods to prepare structurally defective TiO_2 with Ti^{3+} include the partial oxidation of low-valence Ti species (Ti, Ti (II) and Ti (III)), H_2 thermal treatment and the reduction of Ti^{4+} to Ti^{3+} by a chemical reducing agent ($NaBH_4$), metals (Al, Mg, Li, Zn), etc. [44–49]. Although there are numerous preparation methods available, most of them require high consumption of chemicals, as well as multiple steps using specialized equipment. Therefore, it is of significant importance to develop a facile and feasible method to prepare defective TiO_2 with Ti^{3+}.

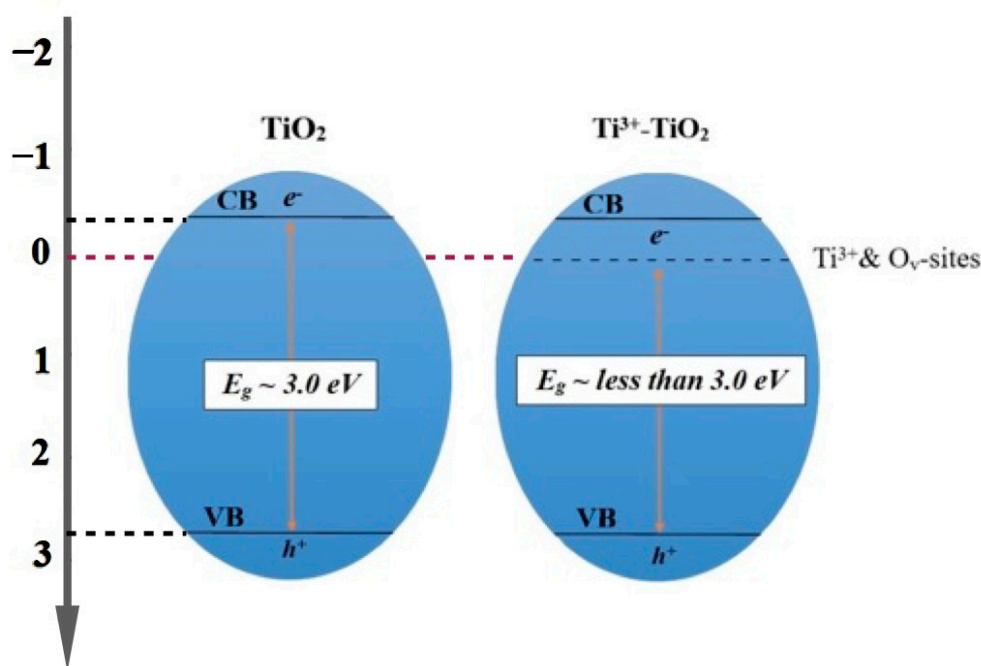**Figure 1.** Schematic showing energy levels of TiO_2 in the presence of Ti^{3+} ions.

In the present work, Ti_2O_3 alone or in combination with TiO_2 (P25) was thermally treated through a simple one-step method, and their photocatalytic performance towards 4-t-BP degradation under simulated solar light was tested. The as-prepared samples were characterized by means of SEM, TEM, BET, XRD, Raman and UV–VIS spectroscopies to study their morphology, textural properties, crystal structure and optical properties. The effects of the presence of humic acid (HA) and inorganic ions (CO_3^{2-}, NO_3^-, Cl^- and HCO_3^-) on 4-t-BP degradation were also investigated.

2. Results and Discussion

2.1. Characterization of Photocatalysts

XRD measurements were conducted to identify the phase structures of the thermally treated Ti_2O_3 and Ti_2O_3/TiO_2 (hereinafter denoted as mTiO) catalysts (Figures 2 and 3). The diffraction peaks at 2θ = 23.823° (012), 33.040° (104), 34.836° (110), 40.219° (113), 48.786° (024), 53.692° (116), 61.42° (214) and 62.64° (300) were attributed to Ti_2O_3 (JCPDS No. 00-043-1033). With the increase in treatment temperature, the intensity of all characteristic peaks corresponding to Ti_2O_3 became weaker in both Ti_2O_3 and mTiO samples. As the temperature further increased to 750 °C, no typical peaks of Ti_2O_3 were observed, indicating the complete transformation of Ti_2O_3 to rutile TiO_2 (JCPDS No. 00-021-1276) [50,51].

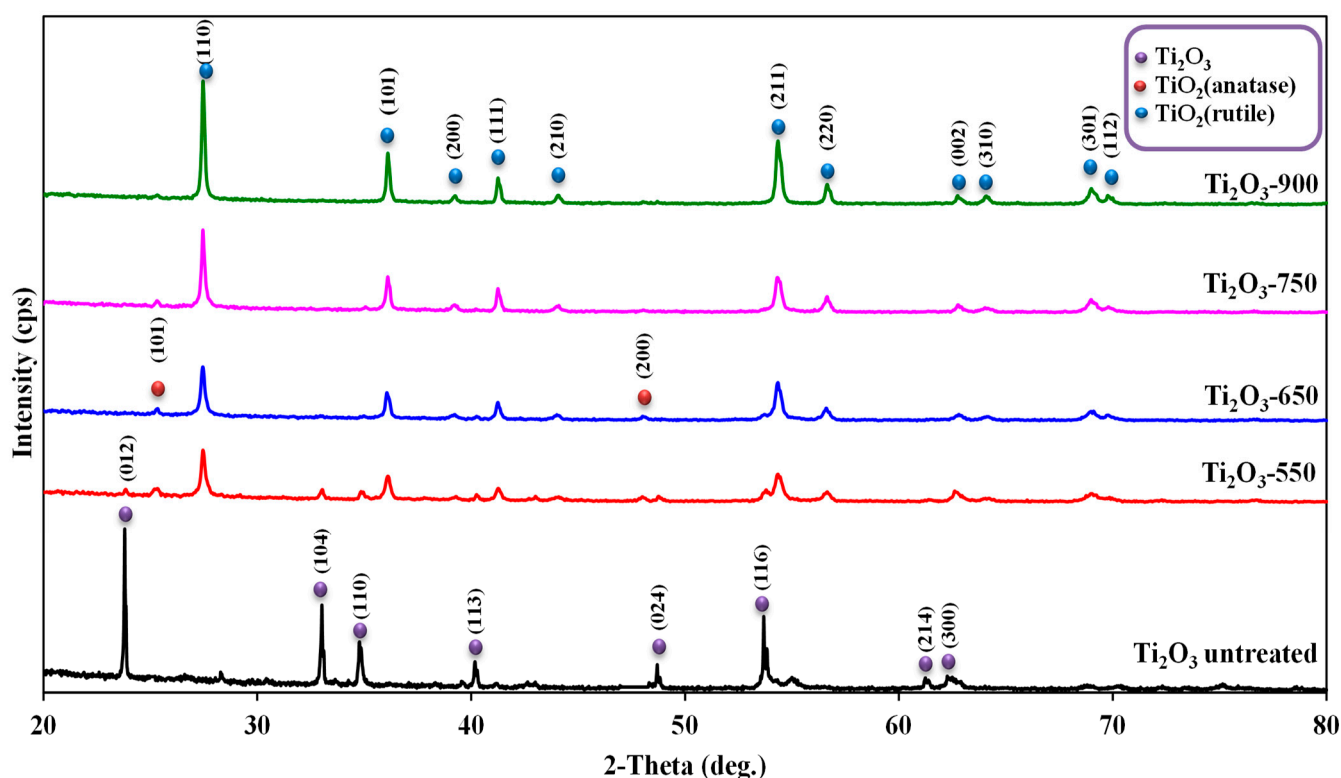**Figure 2.** XRD patterns of treated Ti_2O_3 catalysts.

In the Ti_2O_3-550 sample (Figure 2), apart from the diffraction peaks of TiO_2 rutile, peaks attributed to the anatase phase of TiO_2 (JCPDS No. 00-021-12-72) also appeared at 2θ = 25.3° (101) and 48.028° (200). These findings reveal that the transformation of Ti_2O_3 into TiO_2 anatase also took place. The results are in good agreement with previously reported ones [52]. These peaks almost completely disappeared at 900 °C, suggesting the transformation of TiO_2 anatase into TiO_2 rutile.

The composition of the catalysts was further investigated by Raman spectroscopy (Figures 4 and 5). The Raman peak at around 143 cm^{-1} justified the existence of the TiO_2 anatase phase in both types of catalysts. For treated Ti_2O_3 (Figure 4), this peak became more intense with the increase in treatment temperature to 750 °C, confirming the successful

transformation of Ti_2O_3 into TiO_2 anatase. In addition, low-intensity peaks corresponding to the TiO_2 anatase phase were observed at 196.85 cm^{-1}, 399.57 cm^{-1} and 514.54 cm^{-1} in the spectra of Ti_2O_3-650 and Ti_2O_3-750, while a further increase in temperature to 900 °C led to an increase in the TiO_2 rutile phase. However, no peaks were observed corresponding to Ti_2O_3, which could be attributed to the low intensities of the Raman bands of the Ti_2O_3 structure.
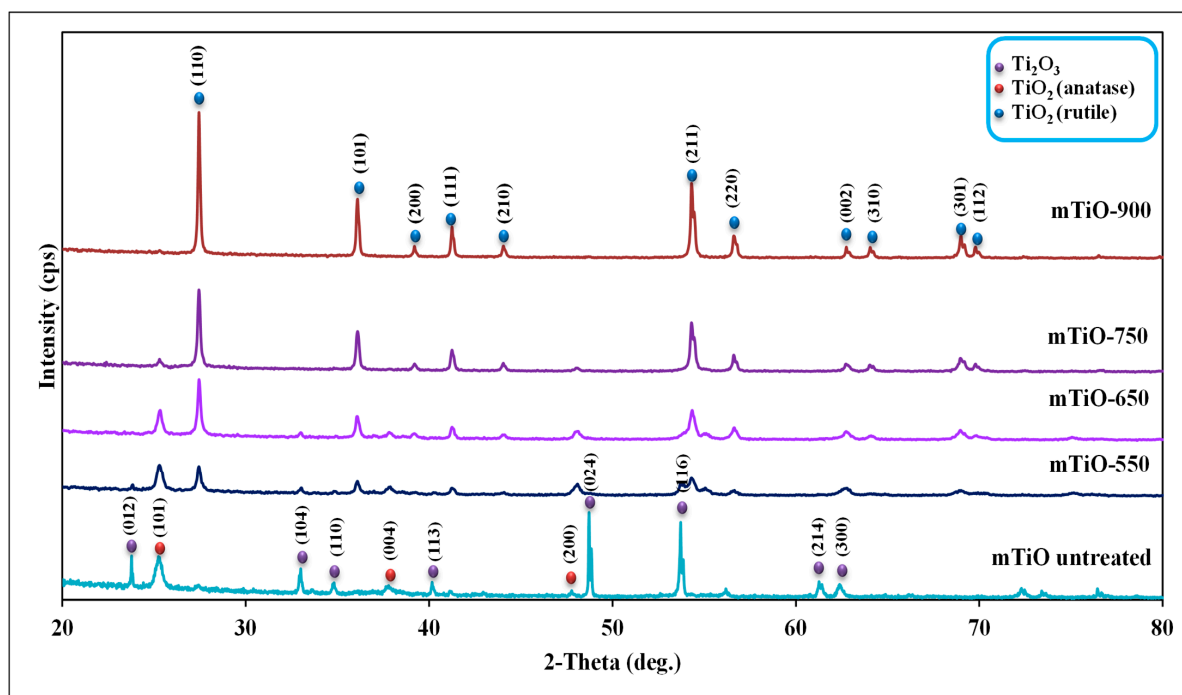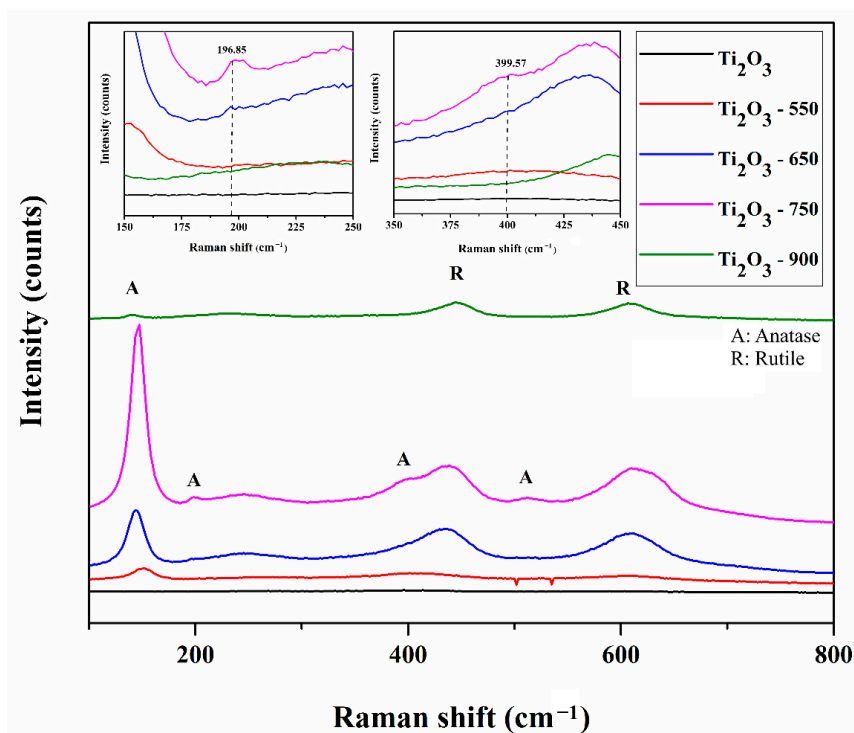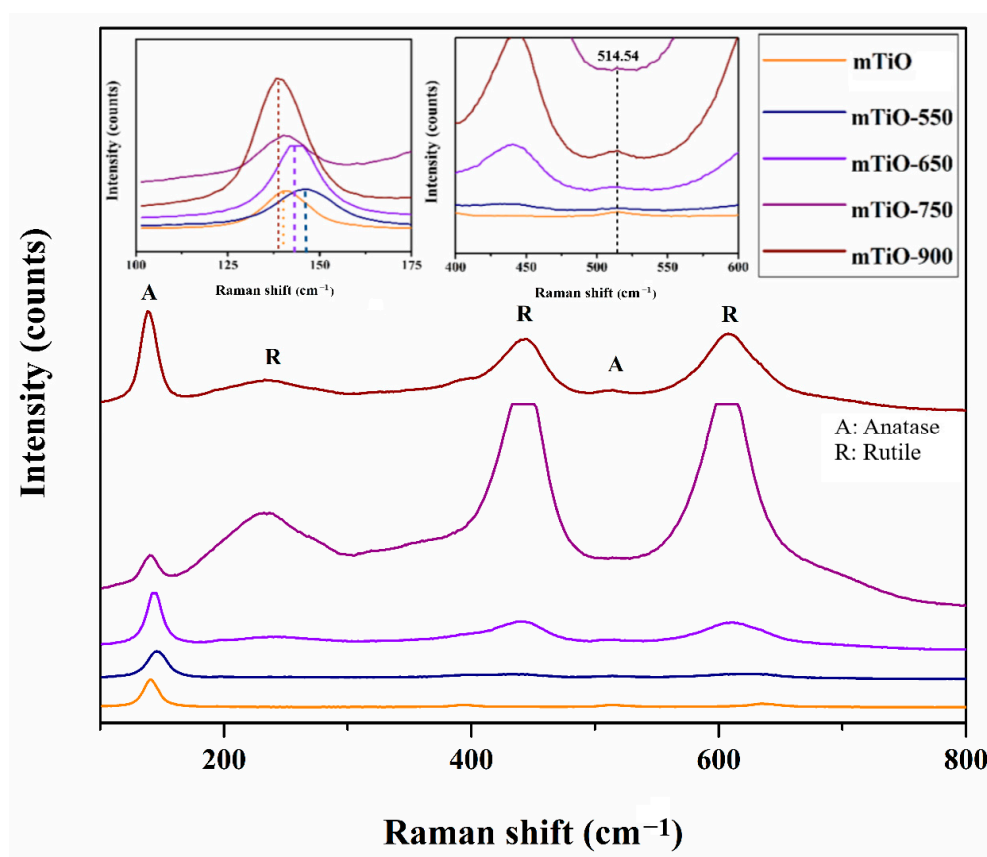

Figure 3. XRD patterns of treated mTiO catalysts.

Figure 4. Raman spectra of treated Ti_2O_3 catalysts.

Figure 5. Raman spectra of treated mTiO catalysts.

Compared to untreated mTiO, mTiO-900 exhibited a negative shift at 143 cm^{-1} (Figure 5), indicating the association of Ti_2O_3 with TiO_2, while, for mTiO-550 and mTiO-650, a positive shift in this peak could possibly be attributed to the introduction of Ti^{3+} and oxygen vacancies into the TiO_2 lattice as a result of the thermal treatment [53]. In the photocatalytic process, the presence of such structural defects in TiO_2 can inhibit the recombination of charge carriers and thus improve the photocatalytic activity.

The results from Raman spectroscopy are in general agreement with the ones obtained from XRD analysis, with the exception of the TiO_2 anatase phase, which was detected only with the first technique for the catalysts treated at 900 °C.

The textural properties of all catalysts were evaluated by BET N_2 adsorption/desorption measurements. As presented in Figures 6 and 7, all the catalysts revealed a typical type-III isotherm according to the classification of the international union of pure and applied chemistry (IUPAC). Interestingly, Ti_2O_3 and mTiO catalysts heated at 650 °C exhibited the highest N_2 adsorption capacity and pore volume (V_p). In general, larger values of V_p can be beneficial for the photocatalytic reaction through providing ionic diffusion and charge transfer on the surface of the photocatalyst [54].

Some other characteristics obtained from the BET analysis are displayed in Table 1, which shows that the treatment temperature had a significant effect on the microstructure of thermally treated Ti_2O_3 and mTiO, particularly on the BET surface area (S_{BET}) and pore volume (Vp). It could be noticed that the S_{BET} of treated Ti_2O_3 was relatively low compared to that of mTiO. The S_{BET} of treated Ti_2O_3 catalysts increased gradually as the treatment temperature increased from 550 °C to 750 °C, which could be likely associated with the formation of a better crystalline framework. However, a further increase in the treatment temperature to 900 °C caused a drastic decrease in S_{BET} due to the phase transformation of TiO_2 anatase to TiO_2 rutile [55].
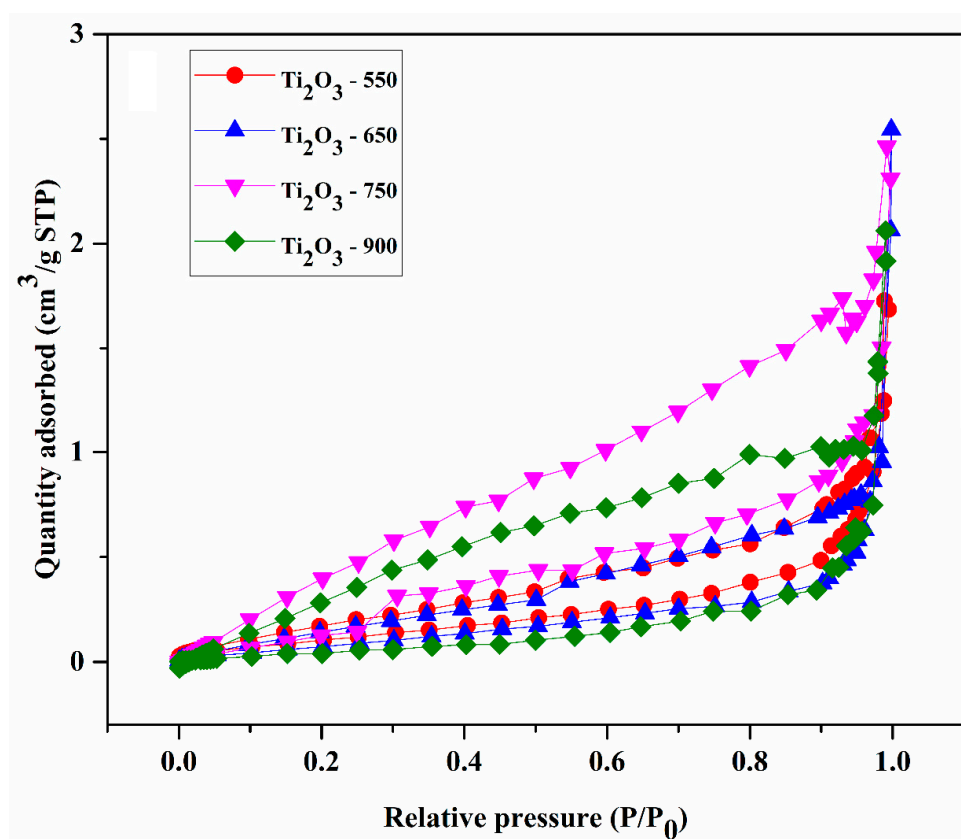
Figure 6. N_2 adsorption/desorption of treated Ti_2O_3 catalysts.
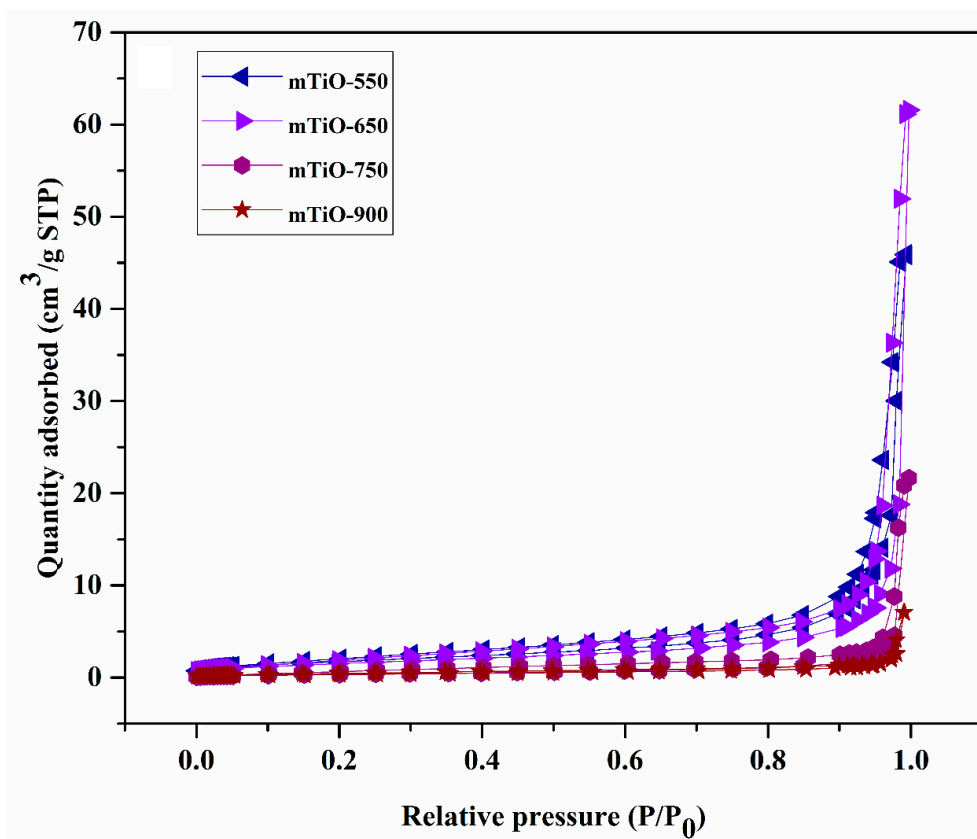

Figure 7. N_2 adsorption/desorption of treated mTiO catalysts.

Table 1. BET surface area and pore volume of as-prepared catalysts.

Photocatalyst	S_{BET} (m^2/g)	V_p (cm^3/g)
Ti$_2$O$_3$-550	1.629	0.009
Ti$_2$O$_3$-650	1.985	0.017
Ti$_2$O$_3$-750	2.733	0.014
Ti$_2$O$_3$-900	0.974	0.012
mTiO-550	23.012	0.255
mTiO-650	20.894	0.347
mTiO-750	5.593	0.134
mTiO-900	3.443	0.029

The increase in treatment temperature continuously decreased the S_{BET} of treated mTiO. The lowering of S_{BET} can be attributed to the increase in particle size as a result of aggregation [56].

The morphology of the prepared catalysts was examined by SEM and TEM. As can be seen from Figure 8, untreated Ti$_2$O$_3$ particles exhibited an irregular shape with a smooth continuous morphology. In contrast, heating under different temperatures resulted in the formation of a much rougher surface of Ti$_2$O$_3$, which could be associated with the phase transformation from Ti$_2$O$_3$ to TiO$_2$ rutile. Such an increase in surface roughness can increase the surface area of the catalyst and further influence the catalytic activity of the material. These results are consistent with the findings obtained from BET analysis, where the heating of Ti$_2$O$_3$ up to 750 °C was accompanied by an increase in S_{BET}.

SEM images of treated mTiO catalysts clearly revealed that thermal treatment caused a particle size growth in TiO$_2$, well-distributed on the surface of Ti$_2$O$_3$ (Figure 9). The increase in the size of TiO$_2$ particles may have resulted in the decrease in S_{BET}.

A UV–VIS absorption study was carried out to assess the light-harvesting ability of the prepared samples (Figures 10 and 11). It can be seen that the temperature variation influenced the light absorption properties of all prepared catalysts. The rise in treatment temperature for Ti$_2$O$_3$ catalysts from 550 °C to 650 °C extended the light absorption to the visible region (400–550 nm), while a further increase in the treatment temperature to 900 °C lowered the visible light absorption capacity (Figure 10).

In contrast, all prepared mTiO catalysts demonstrated a good light absorption ability within the wavelength range of 300−400 nm, although to different extents (Figure 11). Specifically, catalysts heated at lower temperatures demonstrated stronger absorption, which is in accordance with the expectations based on the color change of the catalysts. At the same time, mTiO-550 and mTiO-650 were found to be absorbing in the 400–550 nm region. This phenomenon may be attributed to the transformation of Ti$_2$O$_3$ to TiO$_2$ rutile, containing Ti^{3+} (oxygen vacancies) sites [50,56]. It is noteworthy that the light absorption of mTiO-650 in the visible region was substantially enhanced compared with mTiO-550, as a result of the higher concentration of oxygen vacancies in the lattice of TiO$_2$. Such an enhancement in the light absorption is favorable for improving the photoactivity of the material. On the other hand, the intensities at wavelengths higher than approximately 550 nm gradually weakened for mTiO-550 and mTiO-650.

Moreover, the band gap values of the prepared catalysts were estimated using the Kubelka–Munk equation and the corresponding Tauc plots. As illustrated in Figure 12, the calculated direct band gap energies were found to be 1.76, 1.75, 1.79 and 2.69 eV for Ti$_2$O$_3$-550, Ti$_2$O$_3$-650, Ti$_2$O$_3$-750 and Ti$_2$O$_3$-900, respectively. Similar variations in band gap energies were obtained for mTiO catalysts, where mTiO-650 had a lower band gap of 2.01 eV compared to mTiO-550, mTiO-750 and mTiO-900 (Figure 13). These results reveal the possible application of the prepared catalysts in solar-light-driven photocatalytic reactions.
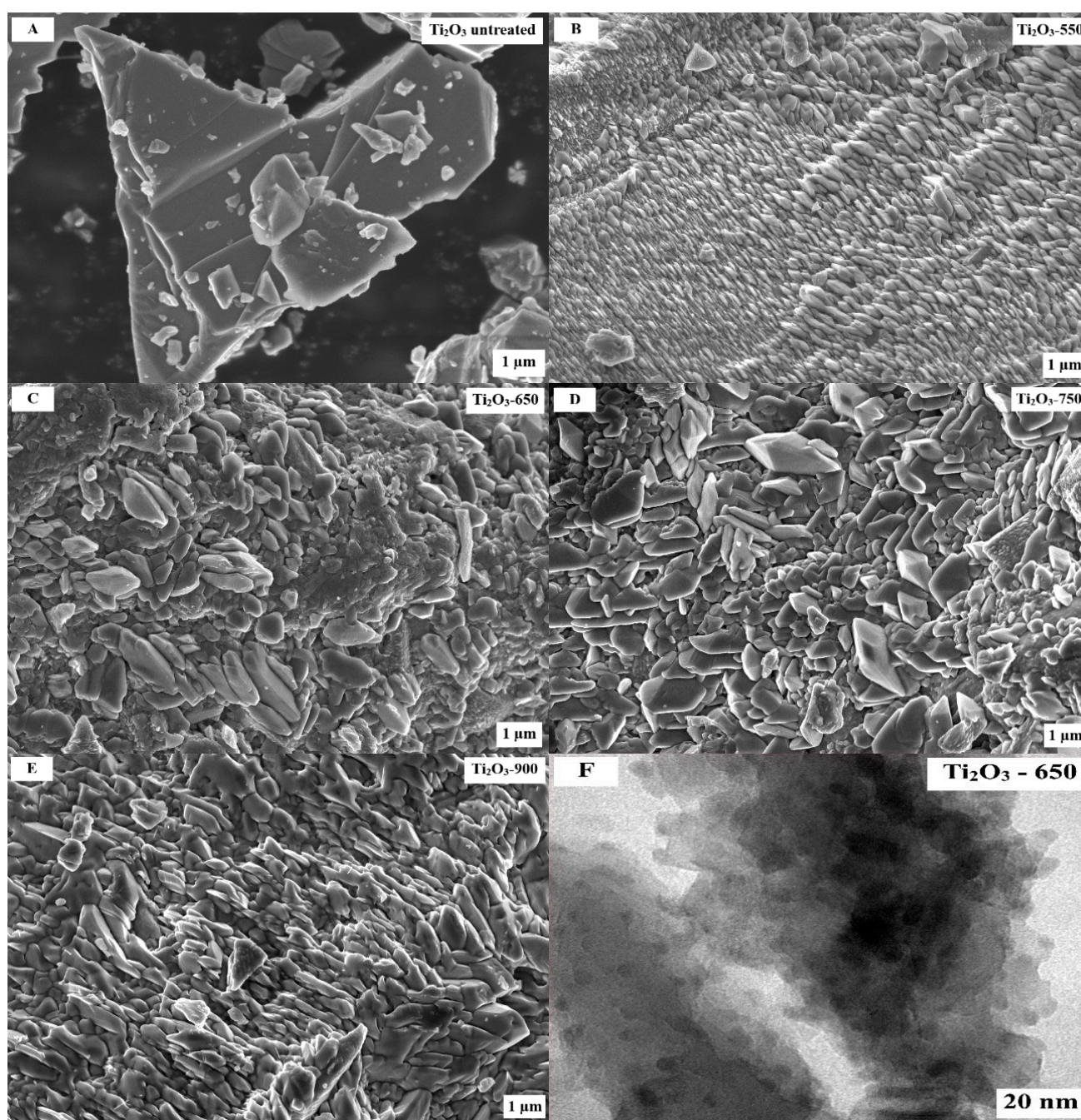
Figure 8. SEM images of Ti$_2$O$_3$ untreated (**A**), Ti$_2$O$_3$-550 (**B**), Ti$_2$O$_3$-650 (**C**), Ti$_2$O$_3$-750 (**D**), Ti$_2$O$_3$-900 (**E**) and TEM image of Ti$_2$O$_3$-650 (**F**).
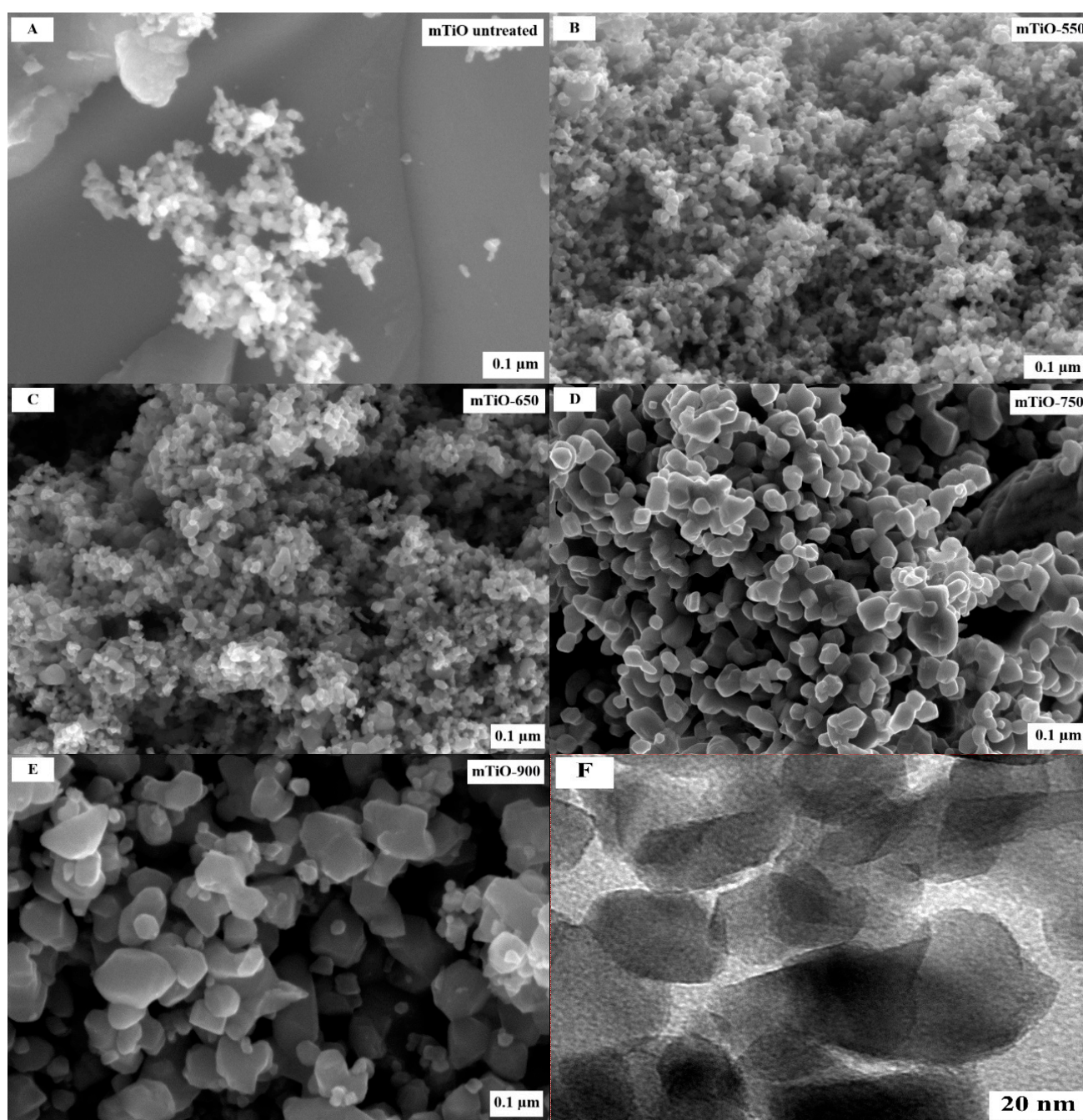
Figure 9. SEM images of mTiO untreated (**A**), mTiO-550 (**B**), mTiO-650 (**C**), mTiO-750 (**D**), mTiO-900 (**E**) and TEM image of mTiO-650 (**F**).
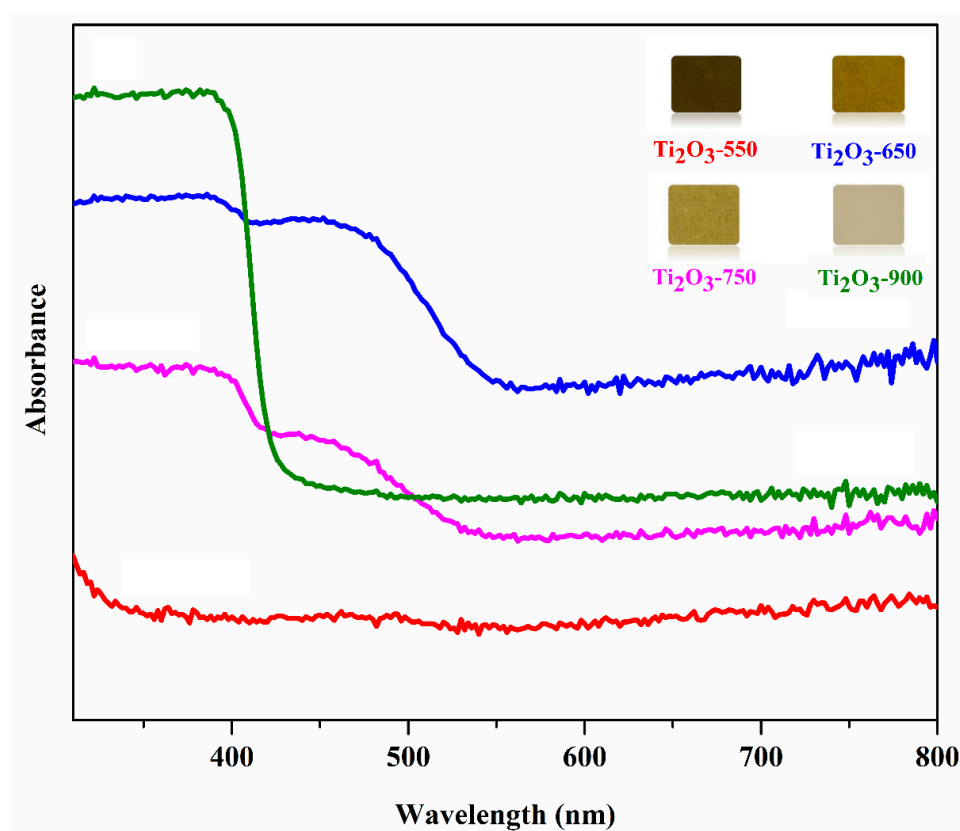
Figure 10. UV–VIS spectra of treated Ti_2O_3 catalysts.
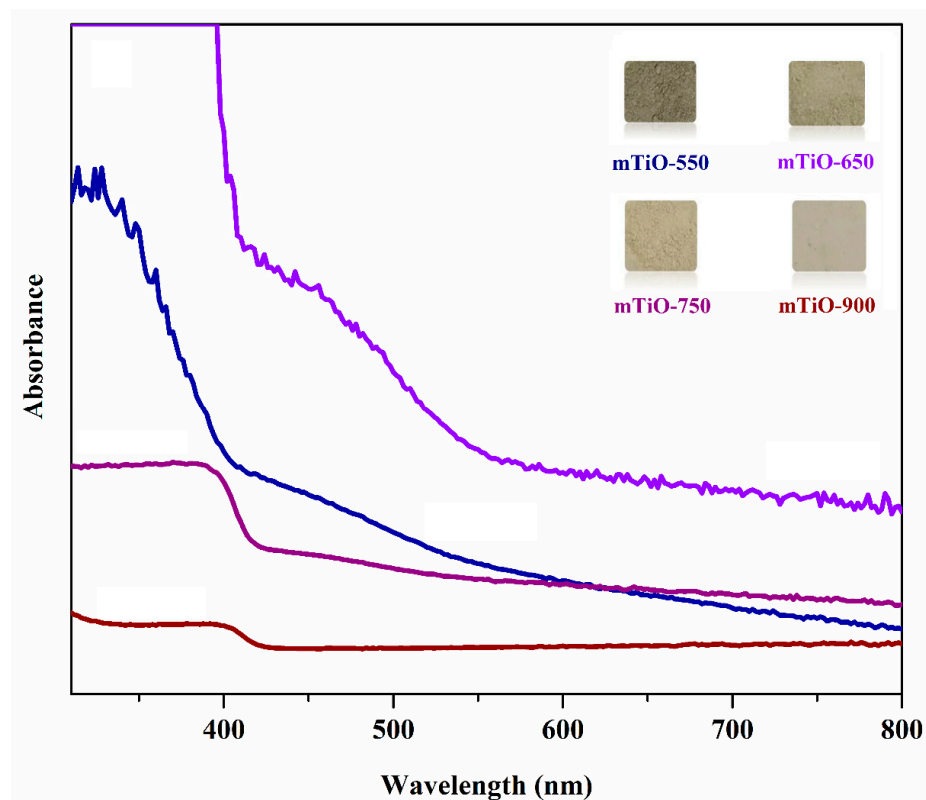
Figure 11. UV–VIS spectra of treated mTiO catalysts.
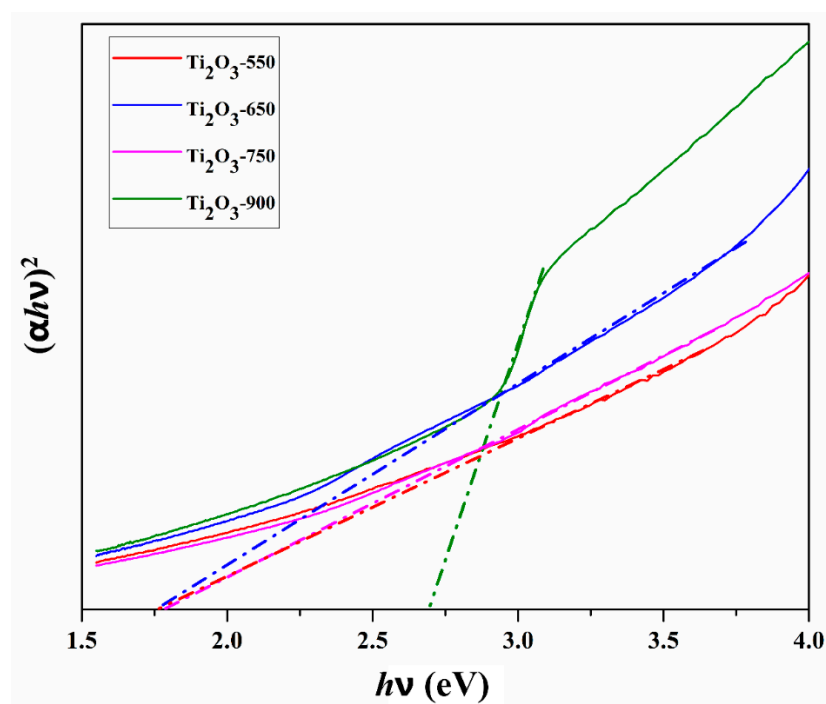
Figure 12. Tauc plot of treated Ti_2O_3 catalysts.
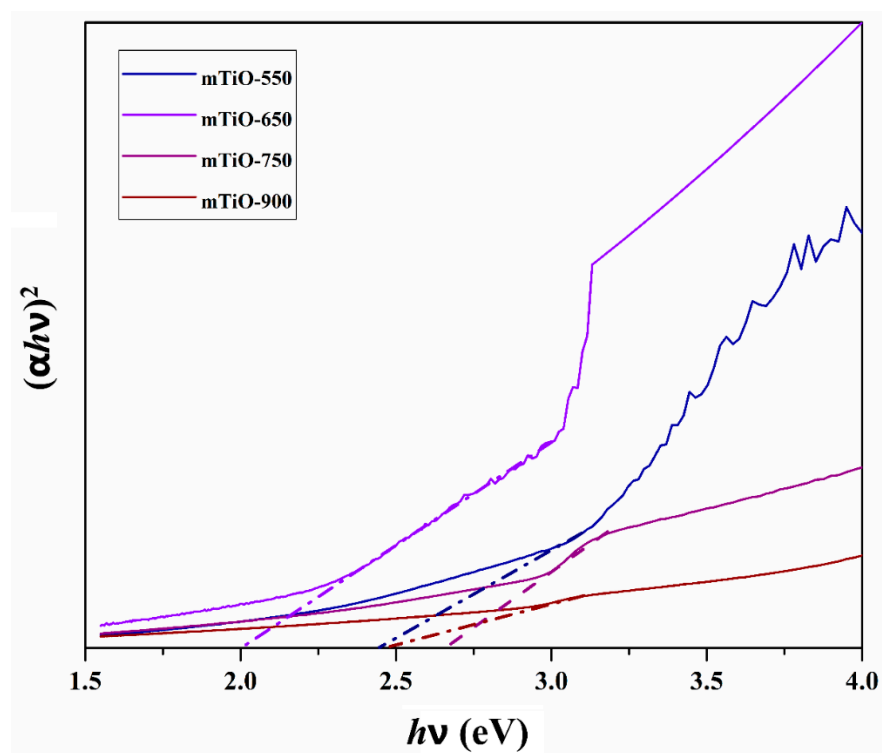
Figure 13. Tauc plot of treated mTiO catalysts.

2.2. Photocatalytic Degradation of 4-t-BP in Aqueous Solution

The photocatalytic activity of all the prepared catalysts was evaluated by the photodegradation of 4-t-BP under solar light irradiation, and the results are shown in Figure 14. In the absence of a catalyst, the decomposition of 4-t-BP observed after 150 min of irradiation was only 8.3%.

Figure 14. The 4-t-BP degradation under solar light irradiation in the presence of prepared catalysts. Reaction conditions: [4-t-BP]$_0$ = 5 mg/L, [photocatalyst] = 200 mg/L.

Treated Ti$_2$O$_3$ showed low photocatalytic activity and approximately 13%, 12.7%, 10.5% and 14% of 4-t-BP was decomposed by Ti$_2$O$_3$-550, Ti$_2$O$_3$-650, Ti$_2$O$_3$-750 and Ti$_2$O$_3$-900, respectively, after 150 min of irradiation. In contrast, mTiO exhibited much higher 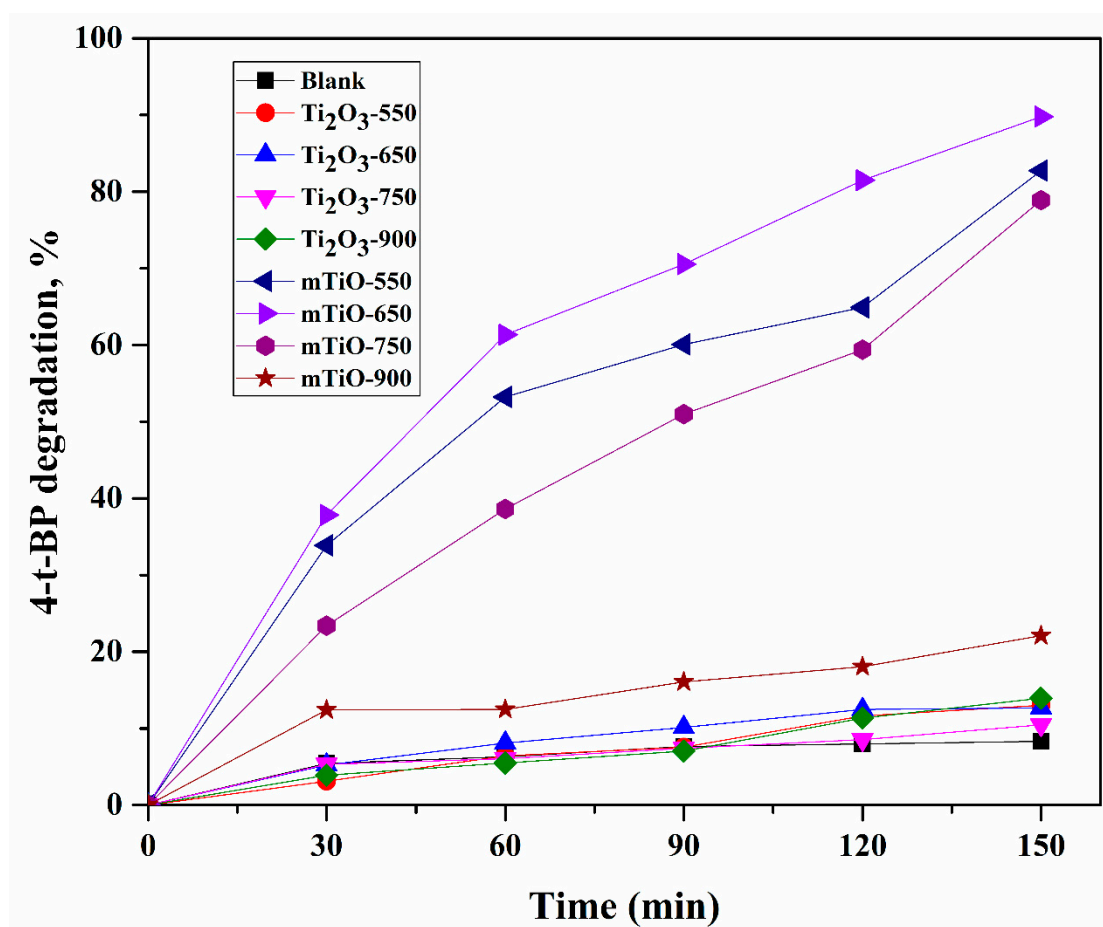photocatalytic degradation efficiency. Among mTiO catalysts, mTiO-650 showed the highest photocatalytic activity, achieving 89.8% of 4-t-BP degradation. These findings are consistent with the results obtained from physico-chemical characterization, where mTiO-650 exhibited better optical properties and a lower band gap and pore volume as compared to mTiO-550, mTiO-750 and mTiO-900, indicating the importance of the treatment temperature on the optical properties and photocatalytic activity of the catalyst [57].

The mineralization efficiency of a photocatalyst is an important indicator for assessing its practical application. Thus, the mineralization of 4-t-BP was evaluated via total organic carbon (TOC) measurements (Figure 15). As in the case of 4-t-BP photodegradation, the treated mTiO catalysts exhibited higher TOC removal than Ti$_2$O$_3$ catalysts. In particular, 54.2% of TOC removal was obtained in 150 min using mTiO-650 under solar light irradiation. In the same reaction time, 32.5%, 12.4%, 12.2%, 11.2%, 10%, 7.8% and 5.4% of TOC removal was obtained for mTiO-550, mTiO-900, mTiO-750, Ti$_2$O$_3$-750, Ti$_2$O$_3$-900, Ti$_2$O$_3$-650 and Ti$_2$O$_3$-550. The observed photocatalytic efficiency of the catalysts tested for TOC removal was in accordance with the 4-t-BP photodegradation results.
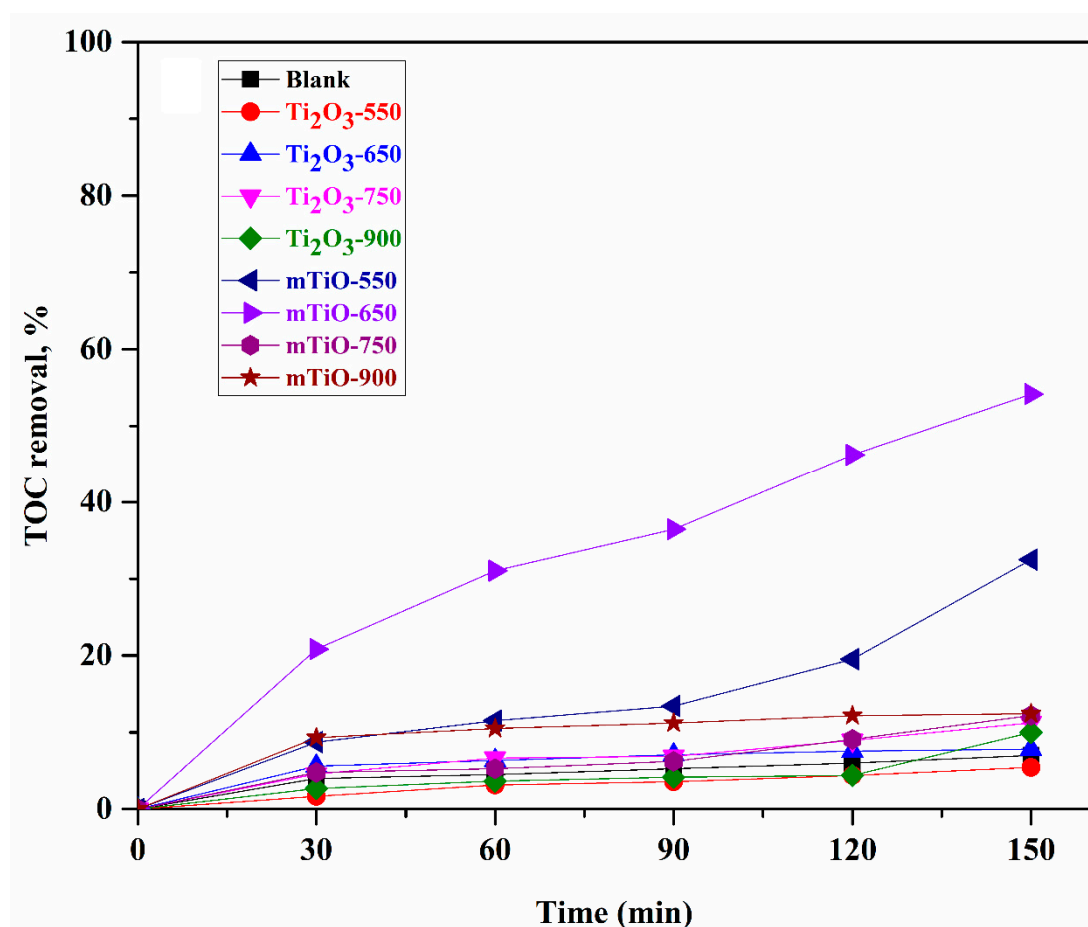
Figure 15. TOC removal under solar light irradiation in the presence of prepared catalysts. [4-t-BP]$_0$ = 5 mg/L, [photocatalyst] = 200 mg/L.

2.3. Effect of HA and Coexisting Ions (CO_3^{2-}, NO_3^-, Cl^- and HCO_3^-) on the Degradation of 4-t-BP
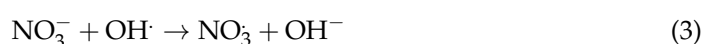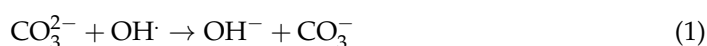
The widespread water constituents in wastewater, including natural organic matter (NOM) and inorganic ions (CO_3^{2-}, NO_3^-, Cl^- and HCO_3^-), could significantly affect the performance of the reaction system towards the degradation and mineralization of the target pollutants [58,59].

NOM is considered an integral part of natural water bodies and wastewater, and it is mainly composed of humic compounds and proteins [60,61]. In this study, HA was used as a model NOM compound and the effects of different concentrations of HA (1 mg/L, 5 mg/L and 10 mg/L) on the degradation of 4-t-BP were investigated. As shown in Figure 16, the presence of HA in the mTiO-650/solar light system could promote or hinder the degradation of 4-t-BP, depending on its concentration. The presence of a relatively low concentration (1 mg/L) of HA increased the degradation efficiency of 4-t-BP from 89.8% to 92.4%, while higher concentrations (5mg/L and 10 mg/L) of HA decreased the degradation efficiency of 4-t-BP to 84.6% and 70.8%, respectively. The enhanced degradation of 4-t-BP in the presence of HA was also observed for the degradation of Bisphenol A [62] and dimethoate [63] by TiO$_2$ photocatalytic degradation. The positive effect of HA at low concentrations might be ascribed to the photosensitization of HA, which would produce extra electrons, leading to an improvement in the photocatalytic degradation of organic pollutants [62,64,65]. On the other hand, at higher concentrations, HA adsorbed on the surface of the catalyst could compete with 4-t-BP for active sites, resulting in a reduction in degradation efficiency [66,67].
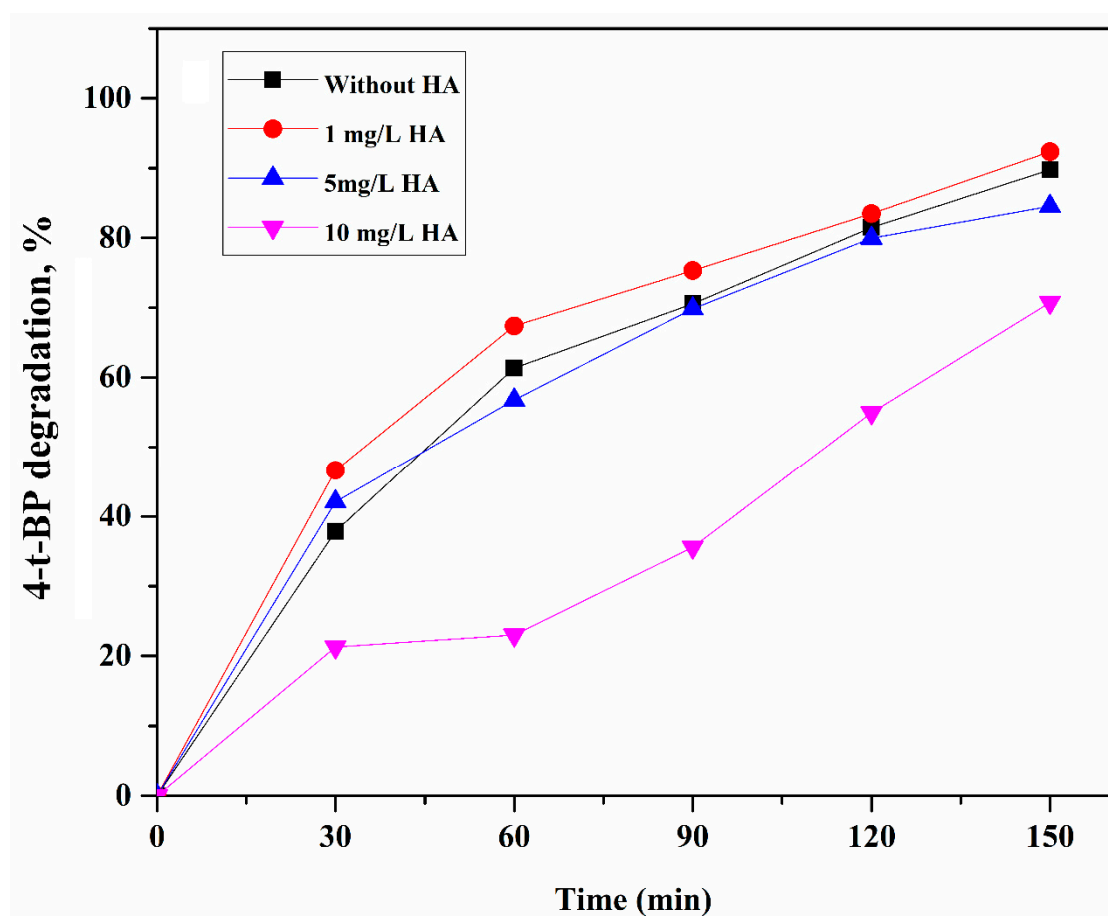
Figure 16. Effects of HA on 4-t-BP degradation under solar irradiation in the presence of mTiO-650. Reaction conditions: [4-t-BP]$_0$ = 5 mg/L, [photocatalyst] = 200 mg/L.
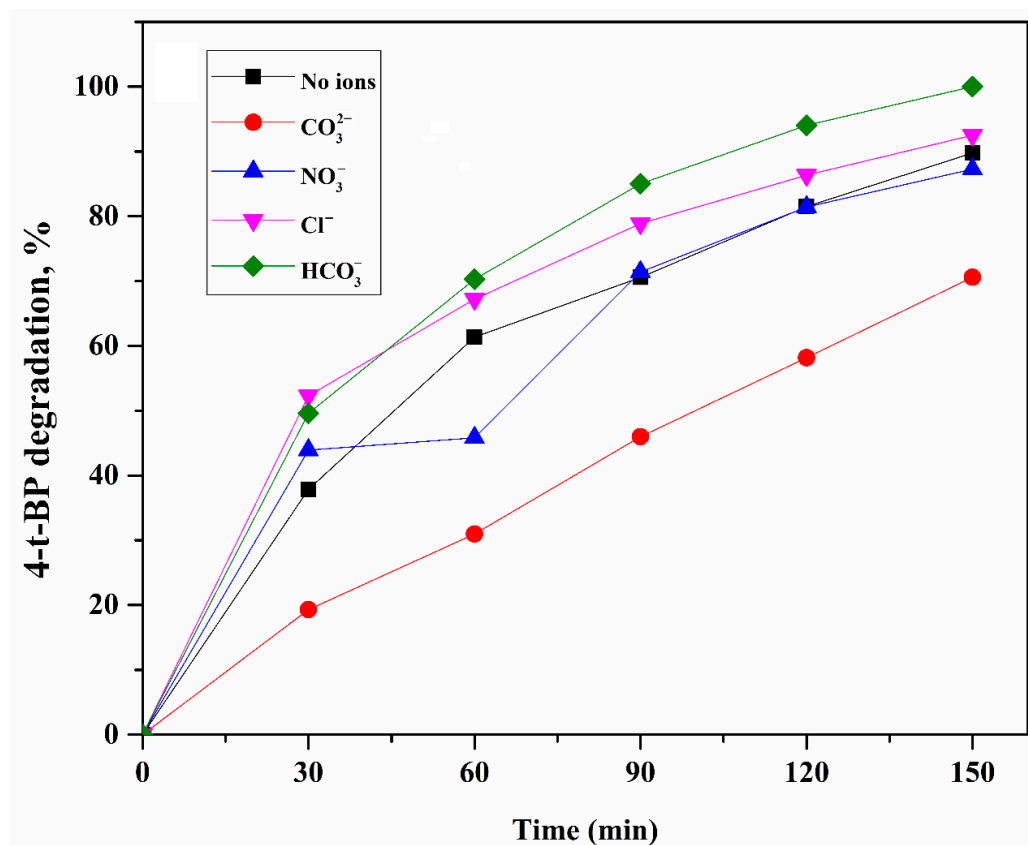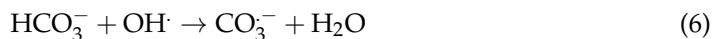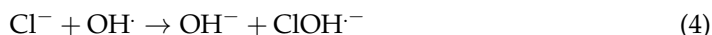
The presence of CO_3^{2-}, NO_3^-, Cl^- and HCO_3^- anions in the concentration of 100 mg/L had dual effects on the degradation of 4-t-BP over mTiO-650. CO_3^{2-} and NO_3^- ions resulted in a certain degree of negative effect with respect to the degradation of 4-t-BP. As shown in Figure 17, the 4-t-BP degradation decreased from 89.8% to 87.3% and 70.3% in the presence of nitrate and carbonate, respectively. The inhibition effect of CO_3^{2-} and NO_3^- was due to: (1) the quenching of oxidizing species, such as hydroxyl radicals (OH·), and positive holes (h$^+$) by anions (Equations (1)–(3)); (2) anions could compete with 4-t-BP molecules for the available active sites of the catalyst surface, which further affects the degradation process [68–71]. Several studies have highlighted that NO_3^- ions are usually weakly adsorbed on the surface of the catalyst and, thus, they slightly inhibit photodegradation reactions [69,72].

$$CO_3^{2-} + OH· \rightarrow OH^- + CO_3^- \tag{1}$$

$$NO_3^- + h_{VB}^+ \rightarrow NO_3 \tag{2}$$

$$NO_3^- + OH· \rightarrow NO_3 + OH^- \tag{3}$$

It is noteworthy that both Cl^- and HCO_3^- accelerated the degradation of 4-t-BP by mTiO-650. The addition of Cl^- and HCO_3^- to the system resulted in 92.5% and 100% degradation after 150 min of solar light irradiation. Cl^- anions reacting with hydroxyl radicals can produce $ClOH^{·-}$ and subsequently transform into $Cl·$ (Equations (4) and (5)) [73]. The generated active chlorine species can selectively attack electron-rich organic compounds [74]. The complete 4-t-BP degradation in the presence of HCO_3^- could be most likely attributed to the generated alkaline condition or the formation of more selective radicals (CO_3^-) by

the reaction of HCO_3^- with $OH\cdot$ (Equation (6)), which can promote the degradation of 4-t-BP [69,75].

$$Cl^- + OH\cdot \rightarrow OH^- + ClOH\cdot^- \tag{4}$$

$$H^+ + ClOH\cdot^- \rightarrow Cl\cdot + H_2O \tag{5}$$

$$HCO_3^- + OH\cdot \rightarrow CO_3^{\cdot-} + H_2O \tag{6}$$

Figure 17. Effects of anions (CO_3^{2-}, NO_3^-, Cl^- and HCO_3^-) on 4-t-BP degradation under solar light irradiation in the presence of mTiO-650. Reaction conditions: [4-t-BP]$_0$ = 5 mg/L, [photocatalyst] = 200 mg/L.

3. Materials and Methods

3.1. Materials

The 4-t-BP (99%), titanium (IV) oxide (TiO$_2$, nanopowder, 21 nm primary particle size, purity $\geq$ 99.5% trace metals basis, P25), titanium (III) oxide (Ti$_2$O$_3$, 100 mesh, 99.9% trace metals basis), Na$_2$CO$_3$, NaNO$_3$, NaCl, NaHCO$_3$ and HA were purchased from Sigma Aldrich. All chemicals were of analytical grade and used as purchased. All aqueous solutions were prepared with ultrapure water (UPW) using a Milli-Q System (18.2 MΩ. cm).

3.2. Preparation of the Photocatalysts

The preparation process was the same for both Ti$_2$O$_3$ alone and mTiO. At first, Ti$_2$O$_3$ or a mixture of Ti$_2$O$_3$ and TiO$_2$ was crushed into a fine powder and then heated in a muffle furnace at 550 °C, 650 °C, 750 °C or 900 °C for 3 h in air. For mTiO, the weight ratio between Ti$_2$O$_3$ and TiO$_2$ was 1:1. The final products were denoted as Ti$_2$O$_3$-X and mTiO-X (with X being the temperature of the thermal treatment), respectively. The detailed synthesis process is illustrated in Figure 18.
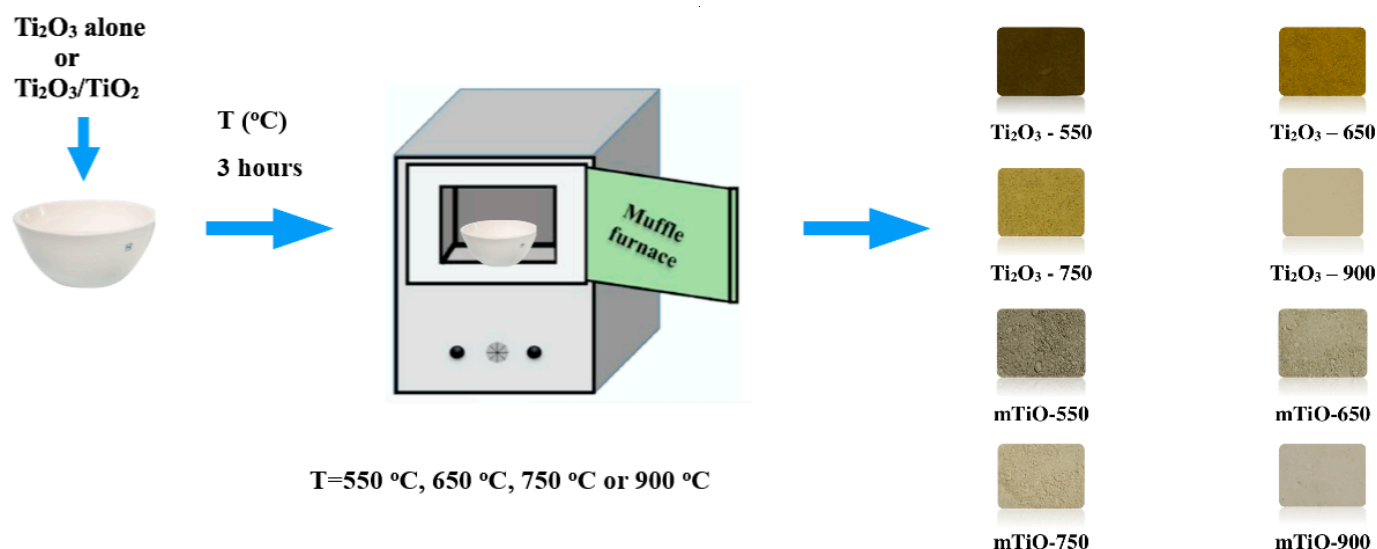
Figure 18. Preparation of thermally treated Ti_2O_3 and mTiO catalysts.

3.3. Characterization of the Photocatalysts

The crystallographic properties and XRD patterns of the prepared catalysts were acquired at 2θ of 20–80° on an X-ray diffraction (XRD, Rigaku Smartlab) system. Raman spectra were recorded with the help of a Raman spectrometer (Horiba, LabRam HR evolution) and excitation energy was λ = 532 nm. Textural properties, including specific surface area (S_{BET}) and pore volume (V_p), were measured using an automated gas sorption analyzer (Autosorb iQ, Quantachrome, Boynton Beach, FL, USA) by the Brunauer–Emmett–Teller (BET) and Barrett–Joyner–Halenda (BJH) method, respectively. Surface morphology was observed by a Scanning Electron Microscope (SEM, Auriga CrossBeam 540, Carl Zeiss) and Transmission Electron Microscope (TEM, JEOL JEM-1400 Plus). UV–VIS spectroscopy of samples was implemented on a Thermo Scientific Genesys 150 UV–Visible spectrophotometer.

3.4. Photodegradation Tests

The photocatalytic performance of the prepared catalysts was evaluated through the experiments of 4-t-BP degradation under simulated solar light irradiation. First, 100 mg of catalyst was added to 500 mL 4-t-BP (5 mg/L) aqueous solution. Prior to irradiation, the mixture was kept in the dark for 15 min under stirring to reach the adsorption/desorption equilibrium. Then, while stirring, the suspension was exposed to the simulated solar irradiation produced by a 100 W Xenon lamp with an AM1.5G filter (LCS-100 solar simulator). During the experiment, 20 mL of reaction solution was extracted at regular time intervals and filtered by a 0.22 μm Millex syringe filter to remove the photocatalyst for further analysis.

The concentration of 4-t-BP was analyzed by a high-performance liquid chromatography instrument (HPLC, Agilent 1290 Infinity II, Santa Clara, CA, USA) equipped with an SB-C8 column (2.1 mm × 100 mm, 1.8 μm). The mobile phase composition was methanol and UPW (50:50, *v/v*), which were mixed to compose the mobile phase. The mineralization of 4-t-BP solution was monitored from the decay of TOC content, measured by a TOC analyzer (Multi N/C 3100, Analytic Jena, Jena, Germany).

4. Conclusions

In summary, Ti_2O_3 and mTiO photocatalysts were prepared via a one-step synthesis method and further characterized by different tests. The effect of treatment temperature on the physicochemical properties and photocatalytic performance of the prepared catalysts in the degradation of 4-t-BP under simulated solar light irradiation was investigated. Based

on the results obtained, the increase in treatment temperature from 550 °C to 650 °C caused an increase in the pore volume and enhanced light absorbance in the visible region (400–550 nm) for both Ti_2O_3 and mTiO photocatalysts. The improved textural and optical properties related to the anatase to rutile ratio and specific surface area contributed to the enhanced performance of mTiO-650, which exhibited the highest photocatalytic activity at the dosage of 0.2 mg/L, achieving 89.8% degradation and 54.2% mineralization of 4-t-BP after 150 min. The effect of treatment temperature on the catalytic performance of the treated Ti_2O_3 catalysts was almost negligible and resulted in 13%, 12.7%, 10.5% and 14% 4-t-BP degradation by Ti_2O_3-550, Ti_2O_3-650, Ti_2O_3-750 and Ti_2O_3-900, respectively. In addition, the effects of the presence of HA and various inorganic ions, including CO_3^{2-}, NO_3^-, Cl^- and HCO_3^- on the photodegradation of 4-t-BP by mTiO-650 were also studied. At relatively low concentrations, HA could act as a photosensitizer and therefore promoted the degradation of 4-t-BP, whereas higher concentrations inhibited the degradation. The presence of Cl^- and HCO_3^- exhibited a positive influence on 4-t-BP degradation, resulting from the favorable formation of additional reactive species, while the presence of NO_3^- and CO_3^{2-} slightly inhibited the reaction.

References

1. Zhang, M.; Dong, H.; Zhao, L.; Wang, D.-X.; Meng, D. A Review on Fenton Process for Organic Wastewater Treatment Based on Optimization Perspective. *Sci. Total Environ.* **2019**, *670*, 110–121. [CrossRef] [PubMed]
2. Yu, X.; Sui, Q.; Lyu, S.; Zhao, W.; Liu, J.; Cai, Z.; Yu, G.; Barcelo, D. Municipal Solid Waste Landfills: An Underestimated Source of PPCPs in the Water Environment. *Environ. Sci. Technol.* **2020**, *54*, 9757–9768. [CrossRef] [PubMed]
3. Yadav, D.; Rangabhashiyam, S.; Verma, P.; Singh, P.; Devi, P.; Kumar, P.; Kumar, K.S. Environmental and Health Impacts of Contaminants of Emerging Concerns: Recent Treatment Challenges and Approaches. *Chemosphere* **2021**, *272*, 129492. [CrossRef]
4. Noguera-Oviedo, K.; Aga, D. Lessons Learned from More than Two Decades of Research on Emerging Contaminants in the Environment. *J. Hazard. Mater.* **2016**, *316*, 242–251. [CrossRef]
5. Ferronato, N.; Torretta, V. Waste Mismanagement in Developing Countries: A Review of Global Issues. *Int. J. Environ. Res. Public Health* **2019**, *16*, 1060. [CrossRef] [PubMed]
6. Fobbe, R.; Kuhlmann, B.; Nolte, J.; Preuß, G.; Skark, C.; Zullei-Seibert, N. Organic Pollutants in the Water Cycle: Properties, Occurrence, Analysis and Environmental Relevance of Polar Compounds. In *Organic Pollutants in the Water Cycle: Properties, Occurrence, Analysis and Environmental Relevance of Polar Compounds*; John Wiley & Sons: Hoboken, NJ, USA, 2006; pp. 121–153. [CrossRef]
7. Peck, A.M. Analytical Methods for the Determination of Persistent Ingredients of Personal Care Products in Environmental Matrices. *Anal. Bioanal. Chem.* **2006**, *386*, 907–939. [CrossRef] [PubMed]
8. Giokas, D.L.; Salvador, A.; Chisvert, A. UV Filters: From Sunscreens to Human Body and the Environment. *TrAC Trends Anal. Chem.* **2007**, *26*, 360–374. [CrossRef]
9. Wang, C.; Shi, H.; Adams, C.D.; Gamagedara, S.; Stayton, I.; Timmons, T.; Ma, Y. Investigation of Pharmaceuticals in Missouri Natural and Drinking Water Using High Performance Liquid Chromatography-Tandem Mass Spectrometry. *Water Res.* **2011**, *45*, 1818–1828. [CrossRef] [PubMed]

10. Lai, W.W.-P.; Lin, J.; Tung, H.-H.; Lo, S.-L.; Lin, A. Occurrence of Pharmaceuticals and Perfluorinated Compounds and Evaluation of the Availability of Reclaimed Water in Kinmen. *Emerg. Contam.* **2016**, *2*, 135–144. [CrossRef]

11. Wanda, E.M.M.; Nyoni, H.; Mamba, B.B.; Msagati, T.A.M. Occurrence of Emerging Micropollutants in Water Systems in Gauteng, Mpumalanga, and North West Provinces, South Africa. *Int. J. Environ. Res. Public Health* **2017**, *14*, E79. [CrossRef]

12. Rivera-Jaimes, J.A.; Postigo, C.; Melgoza-Alemán, R.M.; Aceña, J.; Barceló, D.; López de Alda, M. Study of Pharmaceuticals in Surface and Wastewater from Cuernavaca, Morelos, Mexico: Occurrence and Environmental Risk Assessment. *Sci. Total Environ.* **2018**, *613–614*, 1263–1274. [CrossRef]

13. Nikolaou, A. Pharmaceuticals and Related Compounds as Emerging Pollutants in Water: Analytical Aspects. *Glob. Nest J.* **2013**, *15*, 1–12.

14. Seibert, D.; Quesada, H.; Bergamasco, R.; Borba, F.; Pellenz, L. Presence of Endocrine Disrupting Chemicals in Sanitary Landfill Leachate, Its Treatment and Degradation by Fenton Based Processes: A Review. *Process Saf. Environ. Prot.* **2019**, *131*, 255–267. [CrossRef]

15. Reis, B.; Silveira, A.; Tostes, L.; Okuma, A.; Lange, L.; Amaral, M. Organic Compounds Removal and Toxicity Reduction of Landfill Leachate by Commercial Bakers' Yeast and Conventional Bacteria Based Membrane Bioreactor Integrated with Nanofiltration. *Waste Manag.* **2017**, *70*, 170–180. [CrossRef]

16. Dan, A.; Fujii, D.; Soda, S.; Machimura, T.; Ike, M. Removal of Phenol, Bisphenol A, and 4-Tert-Butylphenol from Synthetic Landfill Leachate by Vertical Flow Constructed Wetlands. *Sci. Total Environ.* **2016**, *578*, 566–576. [CrossRef]

17. Barse, A.V.; Chakrabarti, T.; Ghosh, T.; Pal, A.; Jadhao, S. One-Tenth Dose of LC50 of 4-Tert-Butylphenol Causes Endocrine Disruption and Metabolic Changes in Cyprinus Carpio. *Pestic. Biochem. Physiol.* **2006**, *86*, 172–179. [CrossRef]

18. He, G.; Xing, C.; Xiao, X.; Hu, R.; Zuo, X.; Nan, J. Facile Synthesis of Flower-like $Bi_{12}O_{17}C_{12}/\beta$-$Bi_2O_3$ Composites with Enhanced Visible Light Photocatalytic Performance for the Degradation of 4-Tert-Butylphenol. *Appl. Catal. B Environ.* **2015**, *170*, 1–9. [CrossRef]

19. Xiao, X.; Xing, C.; He, G.; Zuo, X.; Nan, J.; Wang, L. Solvothermal Synthesis of Novel Hierarchical $Bi_4O_5I_2$ Nanoflakes with Highly Visible Light Photocatalytic Performance for the Degradation of 4-Tert-Butylphe. *Appl. Catal. B Environ.* **2014**, *148–149*, 154–163. [CrossRef]

20. Makhatova, A.; Ulykbanova, G.; Sadyk, S.; Sarsenbay, K.; Atabaev, T.; Inglezakis, V.; Poulopoulos, S. Degradation and Mineralization of 4-Tert-Butylphenol in Water Using Fe-Doped TiO_2 Catalysts. *Sci. Rep.* **2019**, *9*, 1–15. [CrossRef] [PubMed]

21. Black & Veatch Corporation. *White's Handbook of Chlorination and Alternative Disinfectants*; John Wiley & Sons, Inc.: Hoboken, NJ, USA, 2009. [CrossRef]

22. Chong, M.N.; Jin, B.; Chow, C.W.K.; Saint, C. Recent Developments in Photocatalytic Water Treatment Technology: A Review. *Water Res.* **2010**, *44*, 2997–3027. [CrossRef]

23. Paździor, K.; Bilińska, L.; Ledakowicz, S. A Review of the Existing and Emerging Technologies in the Combination of AOPs and Biological Processes in Industrial Textile Wastewater Treatment. *Chem. Eng. J.* **2018**, *376*, 120597. [CrossRef]

24. Wang, J.; XU, L. Advanced Oxidation Processes for Wastewater Treatment: Formation of Hydroxyl Radical and Application. *Crit. Rev. Environ. Sci. Technol.* **2012**, *42*, 251–325. [CrossRef]

25. Palmisano, L.; García-López, E.I.; Marcì, G. Inorganic Materials Acting as Heterogeneous Photocatalysts and Catalysts in the Same Reactions. *Dalton Trans.* **2016**, *45*, 11596–11605. [CrossRef]

26. Novak Tusar, N.; Kaucic, V.; Zabukovec Logar, N. Functionalized Porous Silicates as Catalysts for Water and Air Purification. *New Future Dev. Catal. Hybrid Mater. Compos. Organocatalysts* **2013**, 365–383. [CrossRef]

27. Ibhadon, A.O.; Fitzpatrick, P. Heterogeneous Photocatalysis: Recent Advances and Applications. *Catalysts* **2013**, *3*, 189–218. [CrossRef]

28. Siti nor Hidayah, A.; Mohamed, R.; Al-Gheethi, A.; Lai, C.W.; Yashni, G. Heterogeneous Photocatalysis of Triclocarban and Triclosan in Greywater: A Systematic and Bibliometric Review Analysis. *Int. J. Environ. Anal. Chem.* **2021**, *0*, 1–19. [CrossRef]

29. Younis, S.A.; Kim, K.-H. Heterogeneous Photocatalysis Scalability for Environmental Remediation: Opportunities and Challenges. *Catalysts* **2020**, *10*, 1109. [CrossRef]

30. Chen, D.; Cheng, Y.; Zhou, N.; Chen, P.; Wang, Y.; Li, K.; Huo, S.; Cheng, P.; Peng, P.; Zhang, R.; et al. Photocatalytic Degradation of Organic Pollutants Using TiO_2-Based Photocatalysts: A Review. *J. Clean. Prod.* **2020**, *268*, 121725. [CrossRef]

31. Luo, C.; Ren, X.; Dai, Z.; Zhang, Y.; Qi, X.; Pan, C. Present Perspectives of Advanced Characterization Techniques in TiO_2-Based Photocatalysts. *ACS Appl. Mater. Interfaces* **2017**, *9*, 23265–23286. [CrossRef]

32. Chen, J.; Qiu, F.; Xu, W.; Cao, S.; Zhu, H. Recent Progress in Enhancing Photocatalytic Efficiency of TiO_2-Based Materials. *Appl. Catal. Gen.* **2015**, *495*, 131–140. [CrossRef]

33. Ohno, T.; Sarukawa, K.; Tokieda, K.; Matsumura, M. Morphology of a TiO_2 Photocatalyst (Degussa, P-25) Consisting of Anatase and Rutile Crystalline Phases. *J. Catal.* **2001**, *203*, 82–86. [CrossRef]

34. Sangchay, W.; Sikong, L.; Kooptarnond, K. Comparison of Photocatalytic Reaction of Commercial P25 and Synthetic TiO_2-AgCl Nanoparticles. *Procedia Eng.* **2012**, *32*, 590–596. [CrossRef]

35. Obaid, D. Bulk TiO_2 vs alternative Ti-based photocatalysts for the mild aerobic oxidation of alcohols. Ph.D. Thesis, Université Pierre et Marie Curie-Paris VI, Paris, France, 2017.

36. Khan, H.; Swati, I.K. Fe^{3+}-Doped Anatase TiO_2 with d–d Transition, Oxygen Vacancies and Ti^{3+} Centers: Synthesis, Characterization, UV–Vis Photocatalytic and Mechanistic Studies. *Ind. Eng. Chem. Res.* **2016**, *55*, 6619–6633. [CrossRef]

37. Karthik, P.M.; Vinesh, V.; Shaheer, A.R.M.; Neppolian, B. Self-Doping of Ti^{3+} in TiO$_2$ through Incomplete Hydrolysis of Titanium (IV) Isopropoxide: An Efficient Visible Light Sonophotocatalyst for Organic Pollutants Degradation. *Appl. Catal. Gen.* **2019**, *585*, 117208. [CrossRef]

38. Zhang, Q.; Wang, Y.; Zhu, X.; Liu, X.; Li, H. 1T and 2H Mixed Phase MoS$_2$ Nanobelts Coupled with Ti^{3+} Self-Doped TiO$_2$ Nanosheets for Enhanced Photocatalytic Degradation of RhB under Visible Light. *Appl. Surf. Sci.* **2021**, *556*, 149768. [CrossRef]

39. Wu, C.; Gao, Z.; Gao, S.; Wang, Q.; Xu, H.; Wang, Z.; Huang, B.; Dai, Y. Ti^{3+} Self-Doped TiO$_2$ Photoelectrodes for Photoelectrochemical Water Splitting and Photoelectrocatalytic Pollutant Degradation. *J. Energy Chem.* **2016**, *25*, 726–733. [CrossRef]

40. Li, G.; Li, J.; Li, G.; Jiang, G. N and Ti^{3+} Co-Doped 3D Anatase TiO$_2$ Superstructures Composed of Ultrathin Nanosheets with Enhanced Visible Light Photocatalytic Activity. *J. Mater. Chem. A* **2015**, *3*, 22073–22080. [CrossRef]

41. Randorn, C.; Irvine, J.T.S. Synthesis and Visible Light Photoactivity of a High Temperature Stable Yellow TiO$_2$ Photocatalyst. *J. Mater. Chem.* **2010**, *20*, 8700–8704. [CrossRef]

42. Xiu, Z.; Guo, M.; Zhao, T.; Pan, K.; Xing, Z.; Li, Z.; Zhou, W. Recent Advances in Ti^{3+} Self-Doped Nanostructured TiO$_2$ Visible Light Photocatalysts for Environmental and Energy Applications. *Chem. Eng. J.* **2019**, *382*, 123011. [CrossRef]

43. Ghosh, N.G.; Sarkar, A.; Zade, S.S. The Type-II n-n Inorganic/Organic Nano-Heterojunction of Ti^{3+} Self-Doped TiO$_2$ Nanorods and Conjugated Co-Polymers for Photoelectrochemical Water Splitting and Photocatalytic Dye Degradation. *Chem. Eng. J.* **2021**, *407*, 127227. [CrossRef]

44. Zheng, Z.; Huang, B.; Meng, X.; Wang, J.; Wang, S.; Lou, Z.; Wang, Z.; Qin, X.; Zhang, X.; Dai, Y. Metallic Zinc- Assisted Synthesis of Ti^{3+} Self-Doped TiO$_2$ with Tunable Phase Composition and Visible-Light Photocatalytic Activity. *Chem. Commun. Camb. Engl.* **2012**, *49*, 868–870. [CrossRef]

45. Fang, W.; Xing, M.; Zhang, J. A New Approach to Prepare Ti^{3+} Self-Doped TiO$_2$ via NaBH$_4$ Reduction and Hydrochloric Acid Treatment. *Appl. Catal. B Environ.* **2014**, *160–161*, 240–246. [CrossRef]

46. Wang, Z.; Yang, C.; Lin, T.; Yin, H.; Chen, P.; Wan, D.; Xu, F.; Huang, F.; Lin, J.; Xie, X.; et al. Visible-Light Photocatalytic, Solar Thermal and Photoelectrochemical Properties of Aluminium-Reduced Black Titania. *Energy Environ. Sci.* **2013**, *6*, 3007–3014. [CrossRef]

47. Sinhamahapatra, A.; Jeon, J.-P.; Yu, J.-S. A New Approach to Prepare Highly Active and Stable Black Titania for Visible Light-Assisted Hydrogen Production. *Energy Environ. Sci.* **2015**, *8*, 3539–3544. [CrossRef]

48. Li, G.; Lian, Z.; Li, X.; Xu, Y.; Wang, W.; Zhang, D.; Tian, F.; Li, H. Ionothermal Synthesis of Black Ti^{3+}-Doped Single-Crystal TiO$_2$ as an Active Photocatalyst for Pollutant Degradation and H$_2$ Generation. *J. Mater. Chem. A* **2015**, *3*, 3748–3756. [CrossRef]

49. Liu, X.; Zhu, G.; Wang, G.; Yuan, X.; Lin, T.; Huang, F. Progress in Black Titania: A New Material for Advanced Photocatalysis. *Adv. Energy Mater.* **2016**, *6*, 1600452. [CrossRef]

50. Kako, T.; Umezawa, N.; Xie, K.; Ye, J. Undoped Visible-Light-Sensitive Titania Photocatalyst. *J. Mater. Sci.* **2013**, *48*, 108–114. [CrossRef]

51. Xu, M.; Zada, A.; Yan, R.; Li, H.; Sun, N.; Qu, Y. Ti$_2$O$_3$/TiO$_2$ Heterophase Junctions with Enhanced Charge Separation and Spatially Separated Active Sites for Photocatalytic CO2 Reduction. *Phys. Chem. Chem. Phys.* **2020**, *22*, 4526–4532. [CrossRef] [PubMed]

52. Li, Y.; Yang, Y.; Shu, X.; Wan, D.; Wei, N.; Yu, X.; Breese, M.B.H.; Venkatesan, T.; Xue, J.M.; Liu, Y.; et al. From Titanium Sesquioxide to Titanium Dioxide: Oxidation-Induced Structural, Phase, and Property Evolution. *Chem. Mater.* **2018**, *30*, 4383–4392. [CrossRef]

53. Hardcastle, F.D.; Ishihara, H.; Sharma, R.; Biris, A.S. Photoelectroactivity and Raman Spectroscopy of Anodized Titania (TiO$_2$) Photoactive Water-Splitting Catalysts as a Function of Oxygen- Annealing Temperature. *J. Mater. Chem.* **2011**, *21*, 6337–6345. [CrossRef]

54. Yahya, N.; Aziz, F.; Jaafar, J.; Lau, W.J.; Yusof, N.; Norharyati, W.; Ismail, A.; Aziz, M. Impacts of Annealing Temperature on Morphological, Optical and Photocatalytic Properties of Gel-Combustion-Derived LaFeO3 Nanoparticles. *Arab. J. Sci. Eng.* **2020**, *46*, 6153–6165. [CrossRef]

55. Ji, J.; Xu, Y.; Huang, H.; He, M.; Liu, S.; Liu, G.; Xie, R.; Feng, Q.; Shu, Y.; Zhan, Y.; et al. Mesoporous TiO$_2$ under VUV Irradiation: Enhanced Photocatalytic Oxidation for VOCs Degradation at Room Temperature. *Chem. Eng. J.* **2017**, *327*, 490–499. [CrossRef]

56. Hamdy, M.; Saputera, W.; Groenen, E.; Mul, G. A Novel TiO$_2$ Composite for Photocatalytic Wastewater Treatment. *J. Catal.* **2014**, *310*, 75–83. [CrossRef]

57. Chen, Q.; Liu, H.; Xin, Y.; Cheng, X. TiO$_2$ Nanobelts—Effect of Calcination Temperature on Optical, Photoelectrochemical and Photocatalytic Properties. *Electrochim. Acta* **2013**, *111*, 284–291. [CrossRef]

58. Li, H.; Li, J.; Ai, Z.; Jia, F.; Zhang, L. Oxygen Vacancy-Mediated Photocatalysis of BiOCl: Reactivity, Selectivity and Perspective. *Angew. Chem. Int. Ed. Engl.* **2017**, *57*, 122–138. [CrossRef] [PubMed]

59. Wang, Y.; Ao, Z.; Sun, H.; Duan, X.; Wang, S. Activation of Peroxymonosulfate by Carbonaceous Oxygen Groups: Experimental and Density Functional Theory Calculations. *Appl. Catal. B Environ.* **2016**, *198*, 295–302. [CrossRef]

60. Yang, W.; Bradford, S.; Wang, Y.; Sharma, P.; Shang, J.; Baoguo, L. Transport of Biochar Colloids in Saturated Porous Media in the Presence of Humic Substances or Proteins. *Environ. Pollut.* **2018**, *246*, 855–863. [CrossRef] [PubMed]

61. Wang, X.-X.; Liu, B.-M.; Lu, M.-F.; Li, Y.-P.; Jiang, Y.-Y.; Zhao, M.-X.; Huang, Z.-X.; Pan, Y.; Miao, H.-F.; Ruan, W.-Q. Characterization of Algal Organic Matter as Precursors for Carbonaceous and Nitrogenous Disinfection Byproducts Formation: Comparison with Natural Organic Matter. *J. Environ. Manag.* **2021**, *282*, 111951. [CrossRef]

62. Wu, W.; Guoqiang, S.; Wang, S.; Zhu, L.; Yue, L.; Xiang, Q.; Zhang, Y.; Li, Z. Environmentally Relevant Impacts of Nano-TiO_2 on Abiotic Degradation of Bisphenol A under Sunlight Irradiation. *Environ. Pollut.* **2016**, *216*, 166–172. [CrossRef]

63. Chen, J.; Hu, Z.; Wang, D.; Gao, C.; Ji, R. Photocatalytic Mineralization of Dimethoate in Aqueous Solutions Using TiO_2: Parameters and by-Products Analysis. *Desalination* **2010**, *258*, 28–33. [CrossRef]

64. Cheng, R.; Kang, M.; Shen, Z.-P.; Shi, L.; Zheng, X. Visible-Light-Driven Photocatalytic Inactivation of Bacteriophage F2 by Cu-TiO_2 Nanofibers in the Presence of Humic Acid. *J. Environ. Sci.* **2018**, *77*. [CrossRef]

65. Li, L.; Zheng, X.; Chi, Y.; Wang, Y.; Sun, X.; Yue, Q.; Zhou, W.; Xu, S. Molecularly Imprinted Carbon Nanosheets Supported TiO2: Strong Selectivity and Synergic Adsorption-Photocatalysis for Antibiotics Removal. *J. Hazard. Mater.* **2019**, *383*, 121211. [CrossRef]

66. Wang, M.; Zhang, L.; Guilong, Z.; Pang, T.; Zhang, X.; Cai, D.; Wu, Z. In Situ Degradation of Antibiotic Residues in Medical Intravenous Infusion Bottles Using High Energy Electron Beam Irradiation. *Sci. Rep.* **2017**, *7*, 39928. [CrossRef]

67. Guo, Z.; Zhu, S.; Zhao, Y.; Cao, H.; Liu, F. Radiolytic Decomposition of Ciprofloxacin Using γ Irradiation in Aqueous Solution. *Environ. Sci. Pollut. Res.* **2015**, *22*, 15772–15780. [CrossRef] [PubMed]

68. Ma, B.; Yu, N.; Xin, S.; Xin, Y.; Zhang, C.; Ma, X.; Gao, M. Photoelectrocatalytic Degradation of P-Chloronitrobenzene by g-C_3N_4/TiO_2 Nanotube Arrays Photoelectrodes under Visible Light Irradiation. *Chemosphere* **2021**, *267*, 129242. [CrossRef] [PubMed]

69. Li, J.; Xia, Z.; Ma, D.; Liu, G.; Song, N.; Xiang, D.; Xin, Y.; Zhang, G.; Chen, Q. Improving Photocatalytic Activity by Construction of Immobilized Z-Scheme CdS/Au/TiO_2 Nanobelt Photocatalyst for Eliminating Norfloxacin from Water. *J. Colloid Interface Sci.* **2021**, *586*, 243–256. [CrossRef]

70. Saleh, R.; Taufik, A.; Prakoso, S.P. Fabrication of Ag_2O/TiO_2 Composites on Nanographene Platelets for the Removal of Organic Pollutants: Influence of Oxidants and Inorganic Anions. *Appl. Surf. Sci.* **2019**, *480*, 697–708. [CrossRef]

71. Chládková, B.; Evgenidou, E.; Kvitek, L.; Panacek, A.; Zboril, R.; Kovář, P.; Lambropoulou, D. Adsorption and Photocatalysis of Nanocrystalline TiO_2 Particles for Reactive Red 195 Removal: Effect of Humic Acids, Anions and Scavengers. *Environ. Sci. Pollut. Res. Int.* **2015**, *22*, 16514–16524. [CrossRef] [PubMed]

72. Barka, N.; Qourzal, S.; Assabbane, A.; Nounah, A.; Ait-Ichou, Y. Factors Influencing the Photocatalytic Degradation of Rhodamine B by TiO_2-Coated Non-Woven Paper. *J. Photochem. Photobiol. Chem.* **2008**, *195*, 346–351. [CrossRef]

73. Ziegmann, M.; Doll, T.; Frimmel, F.H. Matrix Effects on the Photocatalytical Degradation of Dichloroacetic Acid and Atrazine in Water. *Acta Hydrochim. Hydrobiol.* **2006**, *34*, 146–154. [CrossRef]

74. Kanakaraju, D.; Motti, C.; Glass, B.; Oelgemöller, M. TiO_2 Photocatalysis of Naproxen: Effect of the Water Matrix, Anions and Diclofenac on Degradation Rates. *Chemosphere* **2015**, *139*, 579–588. [CrossRef] [PubMed]

75. Bekkouche, S.; Merouani, S.; Hamdaoui, O.; Bouhelassa, M. Efficient Photocatalytic Degradation of Safranin O by Integrating Solar-UV/TiO_2/Persulfate Treatment: Implication of Sulfate Radical in the Oxidation Process and Effect of Various Water Matrix Components. *J. Photochem. Photobiol. Chem.* **2017**, *345*, 80–91. [CrossRef]